RAPID COMPUTATION OF BISTATIC SURFACE SCATTERING FROM ROUGH ELASTIC MEDIA

RF Gragg* Naval Research Laboratory, Washington, DC, USA
RJ Soukup Naval Research Laboratory, Washington, DC, USA
RC Gauss Naval Research Laboratory, Washington, DC, USA
D Wurmser Naval Research Laboratory, Washington, DC, USA

1 INTRODUCTION

We have developed an improved general algorithm# for computing the single-frequency, incoherent (i.e. non-specular) scattering strengths of fluid or elastic materials with randomly rough surfaces, specifically those with power-law roughness spectra: $S(k) \propto k^{-\gamma_2}$. This algorithm is physical rather than empirical (i.e., it relates the scattering to measurable geophysical quantities), it accommodates both compressional and shear waves in the target medium, and it is vectorized over in/out scattering directions. Beginning with an improved formulation of small-slope scattering theory, we have produced a new implementation that extends the coverage for the spectral exponent to essentially its full range, $2 < \gamma_2 < 4$. (With earlier techniques, the lower half of that range could not be modeled in this way[12].)

Our area of application is ocean acoustics, and our specific goal has been the accurate modeling of sonar scattering from naturally occurring seafloors (which often have $\gamma_2 < 3$). In that context, we have compared our new algorithm's results to those of perturbation approaches over a wide range of environmental parameter values. We have also validated the algorithm by using it to perform a geoacoustic inversion based on backscatter data from an exposed limestone region of a continental shelf. This work has raised significant issues that are impractical to investigate with further field experiments at sea. To explore them, we are beginning a series of ultrasonic laboratory experiments on man-made model seafloors with specified random roughnesses.

The sonar community's earliest efforts at a quantitative description of the ocean-bottom scattering strength invoked various empirical expressions such as Lambert's rule[1], $\sigma = \mu \sin\theta_{\text{in}} \sin\theta_{\text{out}}$. Although this approach provided a handy way to tabulate and summarize experimental data, it has serious drawbacks: it is workable only within limited angular ranges, it cannot be extrapolated with confidence, and it makes no attempt to include frequency dependence[2]. In short, it is an empirical description, not a physical theory. More recent efforts have invoked the physics of wave propagation and scattering. In the case of elastic media, the primary approach to scattering has been perturbation theory[5]. This approach treats the surface as a featureless plane on which roughness is inscribed in the form of a small perturbation (the relief, $h(x,y)$, is taken to be small relative to the acoustic wavelength, λ). This generally works well with silty sediments, which tend to have negligible shear and small roughness. However, problems arise with stronger bottom materials (e.g. hard sand or rock). For such materials, the small-k components of h can have large amplitudes. The way ahead was shown by Voronovich's introduction of small-slope theory[6,7], which assumes that that the gradient $(\partial h/\partial x, \partial h/\partial y)$ is small but imposes no restriction at all on the size of h itself. This is a more general formulation—a systematic approach that essentially derives a composite-roughness-like theory[4] without the empirical small-k/large-k partitioning of the spectrum that is otherwise required, and

* robert.gragg@nrl.navy.mil
# http://aacs.nrl.navy.mil (Select 'FTP', then 'pub' folder, then 'Scat_Strength' folder.)

which has perturbation theory as a small-*h* asymptotic limit. Small-slope theory, however, originally required Dirichlet boundary conditions. Our algorithm is based on an elegant re-formulation by Dashen and Wurmser[8] and on Wurmser's extension[9] of that formulation to media with completely general elastic properties[#].

In the present work, the incident medium is a fluid, characterized by its density and sound speed, ρ_w and c_w. The target medium, a homogeneous elastic material, is characterized by its density and its compressional and shear sound speeds: ρ_b, c_p, and c_s. Attenuation is provided by allowing small negative imaginary parts in c_p and c_s. The two media are separated by an isotropic rough interface with a power-law spectrum[10],

$$S(k) = \frac{w_2}{(h_0 k)^{\gamma_2}} \qquad \text{for} \qquad k > 0 \tag{1}$$

with strength w_2 and exponent $2 < \gamma_2 < 4$ (corresponding to a fractal dimension[11] between 1 and 2). The physical process responsible for the relevant interaction with the multi-scale roughness of these seafloors is Bragg scattering from those spectral components with wavelengths that approximate λ—the same phenomenon that makes diffraction gratings work. The scattering strength, σ, is the average cross section per unit area, per unit solid angle in the scattered direction.

In the following, we use arrows for 3D vectors and boldface for 2D horizontal vectors; e.g. $\vec{r} = (\boldsymbol{r}, z)$ with $\boldsymbol{r} = (x, y)$. The z axis points upwards. Also, although the sound speeds appear individually, the densities occur only in the ratio $\rho = \rho_b / \rho_w$.

2 ALGORITHM DEVELOPMENT

The theory that we employ yields the scattering strength in the generic separated form that is typical of recent treatments, namely $\sigma = P \times I$, in which P is an algebraic expression that depends on the material properties of the bulk media, and I is a wavenumber integral that involves the spectrum of the interface roughness[10,3]. Both factors also depend on the scattering geometry, but only I is frequency dependent. Our algorithm constitutes an improvement over existing formulations in two respects: (1) P embodies a version of small-slope scattering theory[9] that fully incorporates shear waves in the target medium, (2) I is calculated using a numerical technique devised to cope with the integrand's widely varying rates of oscillation and decay. The final product is a computational algorithm that generates the scattering strengths for all the in/out scattering directions in a single vectorized computation.

As noted above, this algorithm applies to fluid/elastic scattering in general. However, out of a preference for the concrete and familiar, we will hereafter adopt the terminology of ocean acoustics, speaking of the water and seafloor rather than the fluid and elastic media.

2.1 Small-Slope Material Factor, *P*

A downgoing wave in the water has a wavevector $\vec{\kappa} = (\boldsymbol{\kappa}, \kappa_z)$ with a real horizontal component $\boldsymbol{\kappa}$, a negative vertical component κ_z, and $\vec{\kappa} \cdot \vec{\kappa} = K_w^2$ in terms of the water wavenumber $K_w = \omega / c_w$. This wave connects to compressional and shear waves

[#] In fact, Ref. [9] develops a full elastodynamic theory. Shear waves are allowed in the *incident* medium as well, though not in our application.

($u = p,s$) in the bottom having wavevectors $\vec{\kappa}_u = (\boldsymbol{\kappa}, \kappa_{uz})$ with vertical components $\kappa_{uz} = -\sqrt{K_u^2 - |\boldsymbol{\kappa}|^2}$ in which $\vec{\kappa}_u \cdot \vec{\kappa}_u = K_u^2$ in terms of the wavenumbers $K_u = \omega / c_u$. For such $\vec{\kappa}$ vectors, we define the auxiliary functions[9,10]

$$A(\vec{\kappa}) = \rho \frac{\kappa_z}{\kappa_{pz}} \left(1 - 4 \frac{|\boldsymbol{\kappa}|^2}{K_s^2} \frac{\kappa_{sz}}{K_s} \frac{\kappa_{sz} - \kappa_{pz}}{K_s} \right), \quad B(\vec{\kappa}) = \rho \frac{\kappa_z}{\kappa_{pz}} \left(1 - 2 \frac{|\boldsymbol{\kappa}|^2}{K_s^2} \right), \quad C(\vec{\kappa}) = \frac{\kappa_z}{\kappa_{pz}} \left(1 - 2 \frac{\vec{\kappa}_p \cdot \vec{\kappa}_s}{K_s^2} \right).$$

Two important downgoing waves in the water are $\vec{\kappa} = \vec{k}$ and $\vec{\kappa} = -\vec{q}$, where $\vec{k} = (\boldsymbol{k}, k_z)$ and $\vec{q} = (\boldsymbol{q}, q_z)$ are the incident and scattered wavevectors (Fig. 1). The wavevector change due to scattering is $\vec{Q} = \vec{k} - \vec{q} = (\boldsymbol{Q}, Q_z)$.

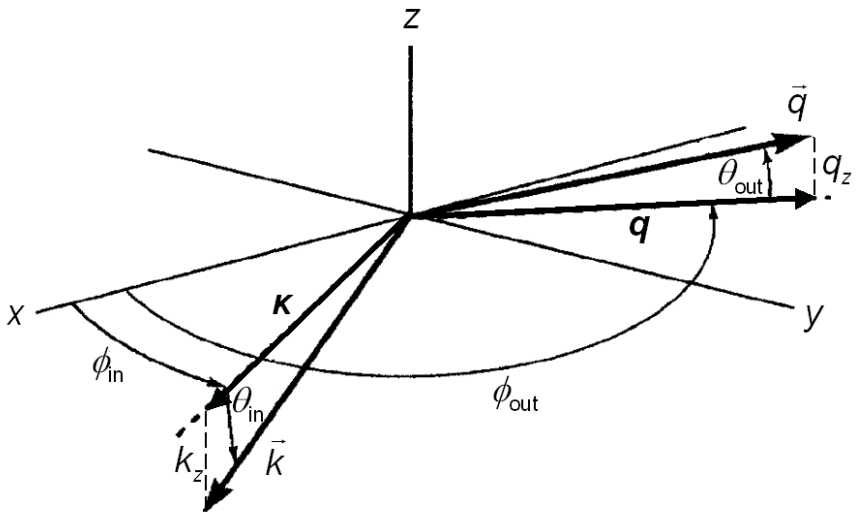

Figure 1. The incident and scattered wavevectors $\vec{k} = (\boldsymbol{k}, k_z)$ and $\vec{q} = (\boldsymbol{q}, q_z)$. These have the same length but different directions: $\vec{k} = K_w \hat{k}$, $\vec{q} = K_w \hat{q}$ in terms of the unit vectors $\hat{k} = \{\theta_{in}, \phi_{in}\}$ and $\hat{q} = \{\theta_{out}, \phi_{out}\}$.

The small-slope expression for the material factor is[9,10]

$$P = \frac{1}{8\pi} \left| \frac{D(\vec{k}, -\vec{q})}{Q_z |\boldsymbol{Q}| [1 + A(\vec{k})][1 + A(-\vec{q})]} \right|^2 \tag{2}$$

where

$$\begin{aligned} D(\vec{k}, -\vec{q}) = {} & 4(1-\rho)[k_z q_z + \boldsymbol{k} \cdot \boldsymbol{q} C(\vec{k}) C(-\vec{q})] + 8\rho [\boldsymbol{k} \cdot \boldsymbol{q} / K_s]^2 \, C(\vec{k}) C(-\vec{q}) \\ & - 4 \boldsymbol{k} \cdot \boldsymbol{q} [A(\vec{k}) - C(\vec{k})][A(-\vec{q}) - C(-\vec{q})] + 4 K_w^2 A(\vec{k}) A(-\vec{q}) \\ & + 2 \rho^{-1} K_s^2 [A(\vec{k}) - B(\vec{k})][A(-\vec{q}) - B(-\vec{q})] - 4 \rho^{-1} K_p^2 B(\vec{k}) B(-\vec{q}) \ . \end{aligned}$$

2.2 Interface Scattering Integral, *I*

We assume that the interface roughness is statistically isotropic; i.e. that there is a dependence on $\phi = \phi_{out} - \phi_{in}$, but not on ϕ_{in} or ϕ_{out} separately. This reduces the scattering integral to the form

$$I = \int_0^\infty J_0(y) y \underbrace{e^{-\alpha y^{2\nu}}}_{B(y;\alpha,\nu)} dy \ , \tag{3}$$

in terms of the dimensionless scaled length $y = |\boldsymbol{Q}| r$, the Lipschitz exponent[11] $\nu = (\gamma_2 - 2)/2$, and a composite parameter

$$\alpha = \frac{\Gamma(1-\nu)}{4^{\nu}\Gamma(1+\nu)} \times \left[\frac{h_{\mathrm{rms}} Q_z}{(h_0 |\boldsymbol{Q}|)^{\nu}} \right]^2 , \tag{4}$$

in which $h_{\mathrm{rms}}^2 = \frac{\pi w_2}{h_0^2} \frac{1}{\nu}$ is the mean-square interface roughness[10]. The same integral appears in other recent formulations as well[3]. Unfortunately, it is unavailable in analytic form except at $\gamma_2 = 3$, the midpoint of the spectral exponent range[10] $2 < \gamma_2 < 4$, and must be evaluated numerically elsewhere. This is particularly challenging because of the oscillation of the Bessel function and the rise of the linear factor, both of which occur at a rate that depends on the scattering geometry, and even more because of the exponential factor $B(y;\alpha,\nu)$ whose highly variable decay rate depends sensitively on the spectral parameters in addition to the geometry*. Heretofore, numerical evaluations have been, with few exceptions, confined to the upper half-range[12] $3 < \gamma_2 < 4$, whereas the lower half is typical of harder seafloors[13,14]. We have developed a numerical algorithm that accurately evaluates (3) for any spectral exponent in the range $2.4 \le \gamma_2 \le 3.9$, which covers virtually all seafloors of practical interest. The computational technique merges two approximate expressions for $B(y;\alpha,\nu)$ (one for small α, the other for large α) that have an overlap in their ranges of validity.

2.2.1 Small α

For small α, the Taylor series $B(y;\alpha,\nu) = \sum_{n=0}^{\infty} (-\alpha y^{\nu})^n / n!$ easily produces an infinite series for I which, when truncated at $n = \tilde{n}$, yields the approximation

$$I = \frac{2}{\pi} \sum_{n=1}^{\tilde{n}} (-)^{n+1} [2^{\nu n} \Gamma(\nu n + 1)]^2 \sin(\nu n \pi) \times \frac{\alpha^n}{n!} \qquad \text{(for small } \alpha\text{)} . \tag{5}$$

At this stage, the appropriate truncation order $\tilde{n}$ is yet to be determined. It is clear, however, that when α is small enough for $\tilde{n} = 1$ to be adequate, one has $I \propto \alpha$, and thus the scattering strength reduces to

$$\sigma = \left| \frac{D(\vec{k}, -\vec{q})}{2[1 + A(\vec{k})][1 + A(-\vec{q})]} \right|^2 \times S(|\boldsymbol{Q}|) . \tag{6}$$

This is the 1st-order *perturbation* result. It applies at the smaller grazing angles and has an $f^{4-\gamma_2}$ frequency dependence.

2.2.2 Large α

For large α (corresponding to the larger grazing angles), we begin with a rational-function approximation to $B(y;\tilde{\alpha},\nu)$ for some *reference* value $\tilde{\alpha}$ of order unity. With $x = y^2$, the approximation of order $[N,D]$ (with $D > N$) is

$$B(y;\tilde{\alpha},\nu) \approx \frac{1 + n_1 x + \cdots + n_N x^N}{1 + d_1 x \cdots + d_D x^D} . \tag{7}$$

The polynomial coefficients $(n_1, \cdots, n_N)$ and $(d_1, \cdots, d_D)$ are determined by fitting the right-hand side of (7) to $B(\sqrt{x};\tilde{\alpha},\nu)$ at a set of points $(x_1, \cdots, x_{N+D})$. (The full specifics about how

* A typical range of interest for backscatter at a few kilohertz is $10^{-3} < \alpha < 10^2$.

these points are chosen, along with other details of the development and testing of this method, are to be found in Refs. [15] and [16].) When the numerator and denominator polynomials are factored, they become $(1-x/z_1)\cdots(1-x/z_N)$ and $(1-x/p_1)\cdots(1-x/p_D)$, respectively, in which z_i and p_j are the zeros and poles. With a little care, this kind of rational-function approximation can be remarkably accurate[17]. The only significant difficulty is that poles or zeros will occasionally fall on the $x>0$ axis. This can be handled with a "splitting" procedure developed by Drumheller[18]. If a pole $p>0$ occurs, first it is split into a complex pair $(pe^{+i\delta}, pe^{-i\delta})$, and then an additional zero[#] $z=p/(2\cos\delta-1)$ is introduced to keep $D-N$ unchanged. In all cases, we find that $\delta=90^\circ$ works well[15,16], so the split poles are simply $(ip,-ip)$ and the additional zero is $-p$. A zero on the real axis is handled in an equivalent way, by splitting the zero and the adding a pole. Once this is done, (7) may be re-written in partial fraction form,

$$B(y;\tilde{\alpha},\nu)=\sum_{m=1}^{D}\frac{r_m}{x-p_m}. \tag{8}$$

With reasonable choices[15,16] for N and D, this gives an excellent approximation to the y dependence of $B(y;\tilde{\alpha},\nu)$ throughout the interval $2.4\le\gamma_2\le 3.9$. As it stands, this applies to $\alpha=\tilde{\alpha}$ only; however, it is trivial to extend it to general α by exploiting the scaling behavior: $B(y;\alpha,\nu)=B(sy;\tilde{\alpha},\nu)$, where $s=(\alpha/\tilde{\alpha})^{1/(2\nu)}$. The equivalent result for $B(y;\alpha,\nu)$ is simply the right-hand side of (8) with the residues and poles (r_m,p_m) replaced by $(r_m/s^2, p_m/s^2)$. The general result for I, then, is

$$I=\sum_{m=1}^{D}\frac{r_m}{s^2}\int_0^\infty\frac{J_0(y)y}{y^2-p_m/s^2}\mathrm{d}y.$$

Since $\mathrm{Re}\left(\sqrt{-p_m}\right)>0$ is guaranteed by the pole-splitting procedure, the integral is available in closed form. The final result is

$$I=\sum_{m=1}^{D}\frac{r_m}{s^2}K_0\left(\frac{\sqrt{-p_m}}{s}\right)\qquad\text{(for large }\alpha\text{)}. \tag{9}$$

2.2.3 General α

Two algorithms have been developed for the scattering integral I, depending on the size of the composite parameter α. For small α, (5) should be used, with an appropriate truncation order $\tilde{n}$. For large α, (9) ought to be applied with some appropriate rational function order $[N,D]$. The operational meanings of "large", "small", and what orders are "appropriate" must be determined empirically. This has been done and reported in detail in Ref. [10]. The outcome is that, for properly chosen $\tilde{n}$ and $[N,D]$, the "small" and "large" ranges of α can actually be made to overlap at a value α', so that universal coverage can be provided by simply using (5) for $\alpha<\alpha'$ and (9) for $\alpha'<\alpha$. Specifically, for $\tilde{n}=40$ and $[N,D]=[6,9]$, $\log_{10}\alpha'=-1.7567\gamma_2+4.4926$ works throughout the interval $2.4\le\gamma_2\le 3.9$.

In summary, the scattering strength has the form, $\sigma=P\times I$, with the material factor P obtained from the small-slope expression and the scattering integral I produced by a merger of small-α and large-α approximations. The resulting formulation for σ not only

[#] This expression for z emerges when the right-hand side of (7) and its corresponding factored form are required to have the same behavior as $x\to 0$.

respects reciprocity*, but is also easily vectorizeable over the variables $\theta_{in}, \theta_{out}, \phi$ when implemented in common computing environments such as Matlab.

3 APPLYING THE ALGORITHM

3.1 Initial Validation

Before using our algorithm to analyze experimental data, we validated it against Essen's perturbative formulation[5], which also includes shear. This formulation relies on an alternate scattering integral formulation that can be evaluated analytically, but only for $\gamma_2 = 3$ and $\gamma_2 = 4$. Numerical backscatter comparisons have confirmed that our small-slope predictions coincide with those of the perturbative algorithm in regimes where agreement is expected (namely, at lower grazing angles) in simulations with or without shear, but that sizeable differences can arise at higher grazing angles[10]. This is illustrated in Fig. 2 for rough basalt at 3.5 kHz. Here and in all subsequent simulations, we have set $h_0 = 1$ m (a customary reference value[10]) and fixed the water parameters at typical seawater values. In the figure, we examine the grazing-angle dependence of σ in the backscatter geometry (with $\phi = 180^o$ and $\theta_{in} = \theta_{out}$).

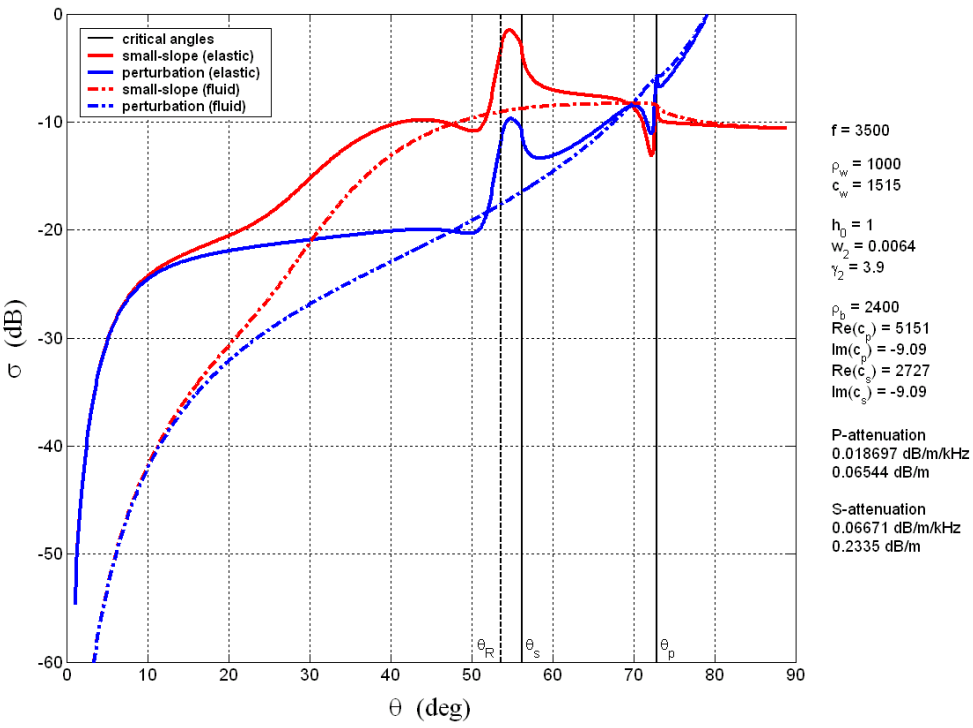

Figure 2. Backscattering strength computations for Essen's rough basalt[5]. The inputs for the "elastic" curves are listed on the right in MKS units. Below these, the attenuations appear in more familiar decibel forms. Small-slope curves are from the algorithm described in the text. Perturbation curves are from (6). The compressional and shear critical angles and the Rayleigh angle are also indicated. "Fluid" curves are produced by "squelching" the shear [via the replacements $\mathrm{Re}(c_s) \to \mathrm{Re}(c_s) \div 10$ and $\mathrm{Im}(c_s) \to \mathrm{Im}(c_s) \times 10$].

* I.e., it is invariant under the interchange[9] $\vec{k} \leftrightarrow -\vec{q}$.

Such model runs have indicated that, for softer sediments, perturbation theory works well up to rather high grazing angles. For some harder seafloors, however, predicting the scattering strength at even moderate grazing angles (roughly $\theta > 20^{o}$ in Fig. 2) requires an algorithm like ours—one that incorporates shear in a small-slope formulation. In addition, in these environments, both theories can exhibit shear-related features that are localized in angle in a way that suggests the generation of interface waves (e.g., the bump in the interval $\theta_{\mathrm{R}} < \theta < \theta_{s}$ in the two "elastic" curves of Fig. 2).

3.2 Field Experiment[13]

With the completion of the initial validation phase, we turned to testing the small-slope scattering algorithm on field data. For this, we processed several data sets gathered during a series of sonar bottom backscattering experiments conducted off the Carolina coast of the United States[19–21]. These experiments were performed in a continental shelf region known to have a limestone seafloor virtually free of any sediment. Beyond the fact of its limestone composition, however, no ground truth was available for the ocean bottom. Since the straightforward option, an unequivocal data-model comparison, was therefore impossible, we attempted a geoacoustic inversion—a controlled search through the 7D environmental parameter space for an optimal data-model fit—as a means of both testing the algorithm and indirectly inferring the in-situ parameter values[22].

To succeed at this, one typically needs the support of a wide range of disparate data, and a rational way to bound the search region in parameter space. These were available in our case. Measurements were made at four different frequencies (2.0, 2.5, 3.0 and 3.5 kHz) and we processed the data to extract scattering strengths for a large spread of grazing angles ($15^{\circ} < \theta < 70^{\circ}$). Though we had no measurements of any of the seven parameters, we did have enough indirect information about them—from published surveys of saturated marine limestones, from the linear theory of elasticity, and from work on similar rough media— to bound the search.

An inversion also requires a cost function to serve as a metric for the data-model mismatch, and an algorithm that can search the parameter space efficiently yet thoroughly. As a cost function we used a simple RMS data-model deviation (computed in decibels, with binned angles, over all four frequencies). We opted for simplicity in the search algorithm as well, choosing the hybrid simplex/annealing strategy "amebsa," available in *Numerical Recipes*[17].

Figure 3 is a typical inversion result. It indicates that the interface scattering algorithm is able to describe the data well for $\theta < \theta_{p}$. In this work, data with $\theta > 70^{o}$ were excluded because they appear to involve scattering by volume inhomogeneities in the material beneath the interface—a process that the present algorithm is not designed to model. Efforts are underway at NRL to remedy this.

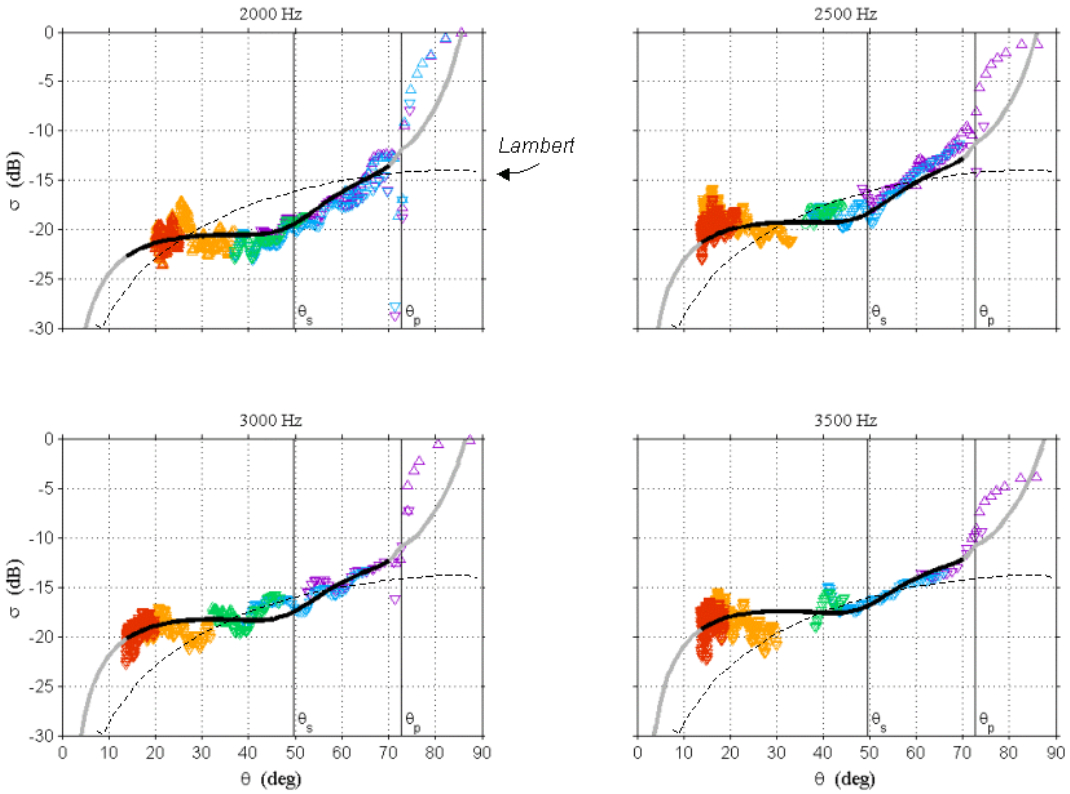

Figure 3. A data-model fit from the limestone geoacoustic inversion (which was done simultaneously over the four experimental frequencies shown). The solid lines at each frequency are the output of the small-slope interface scattering algorithm (black in the θ interval where the fit was computed, gray elsewhere). The symbols are the experimental data[13]. Their colors, which correspond to different beams for the receiving array, are not relevant here[13]. The prediction of Lambert's rule, $\sigma = \mu \sin^2 \theta$ with $\mu = -27$ dB, is also included for comparison, though it is clearly inadequate here. The compressional and shear critical angles are also shown. (This limestone had no Rayleigh angle.)

Of course, because the inversion is a stochastic procedure, it does not produce precisely reproducible results. Figure 3 is typical but not strictly unique. We re-ran the whole inversion process several dozen times and compiled statistics in an effort to see how reliably the values of the various parameters were being extracted. In fact, we did this separately for two different experimental sites[13] (designated Q and C) roughly 7 miles apart. The results are summarized in Fig. 4. At each site, the two interface roughness parameters and the compressional/shear sound speed ratio[#] (w_2, γ_2, ξ) were extracted very reliably. The same might also be said for the shear attenuation, $\mathrm{Im}(c_s)$. The remaining three parameters had such large standard deviations that they were, in effect, uniformly distributed over their search intervals and thus could not be determined at all. We infer that the influence of these parameters on the scattering is weak enough to be masked by experimental uncertainty. By comparing the means and standard deviations for sites Q and C, one can also conclude that the bottom material at these two sites is essentially the same limestone, though its surficial roughness is different.

[#] $\xi = \mathrm{Re}(c_p)/\mathrm{Re}(c_s)$ was used as an environmental parameter rather than $\mathrm{Re}(c_s)$ itself. See Ref. [13] for details.

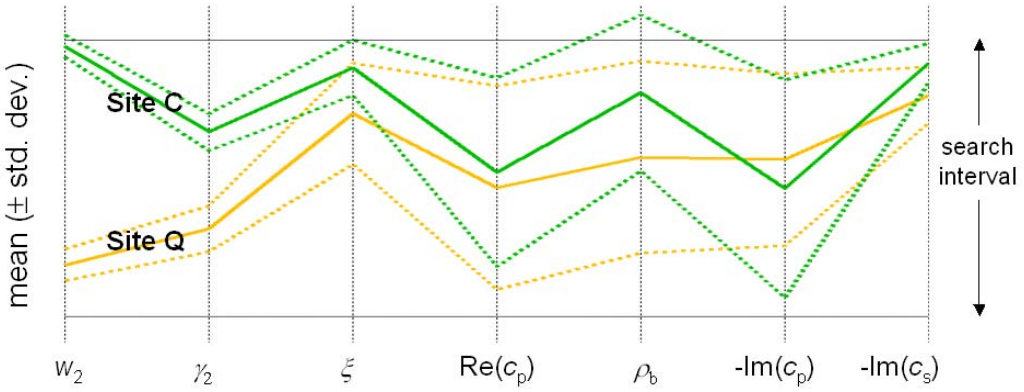

Figure 4. Mean and standard deviation for each of the seven environmental parameters extracted through inversion at the two experimental sites[13]. The parameters' search intervals are all normalized to the same size for display. A parameter whose standard deviation is a small fraction of its search interval is considered to be reliably extracted. A parameter whose mean values from the two sites are within a standard deviation of each other can be considered to have the same value at both sites.

This study has provided further support for our small-slope algorithm as a valid, physics-based tool for modelling interface scattering. However, inversion results like these can never be absolutely conclusive. That kind of closure calls for a carefully controlled experiment with accurate knowledge of the target material's geoacoustic parameters and roughness. Since it is too expensive to conduct such an experiment at sea, scale-model laboratory experiments are indicated.

3.3 Laboratory Experiments

In October 2003, we will begin a series of such experiments in the Naval Research Laboratory's Shallow Water Acoustic Laboratory*. These are to be conducted at ultrasonic frequencies (~300 kHz, typically) on man-made samples with well-known material properties (PVC, for example). These samples (~1 m on a side) will be milled to create rough surfaces corresponding to realizations from carefully prescribed spectra. Figure 5 shows an early version.

In contrast to the seagoing experiments reported above, scattering-strength measurements will not be confined to the backscatter direction. Data will be recorded on hydrophones that can be positioned with freedom in three dimensions, enabling us to examine the full angular dependence of σ. We intend to use the data to complete a definitive validation of the small-slope algorithm, including an investigation of potential surface-wave phenomena that have been suggested by the computer simulations; e.g., the angular pattern seen in Fig. 6. This pattern of strong scattering both for $\theta_{out} \approx \theta_{in}$ in the back direction and for small θ_{out} in the forward direction seems characteristic of situations in which $\theta_{in} \approx \theta_R$, and we suspect that it accompanies the scattering of leaky Stonely waves along the interface[23].

* http://tid-www.nrl.navy.mil/pubs%20pdfs/2001Facilities.pdf (page 111).

Figure 5. Model rough seafloor made of PVC. The dimensions are roughly $1\,\mathrm{m}\times 1\,\mathrm{m}\times 10\,\mathrm{cm}$. (Courtesy, Dr. R. W. Wiley, Allied Geophysical Laboratory/ University of Houston.)

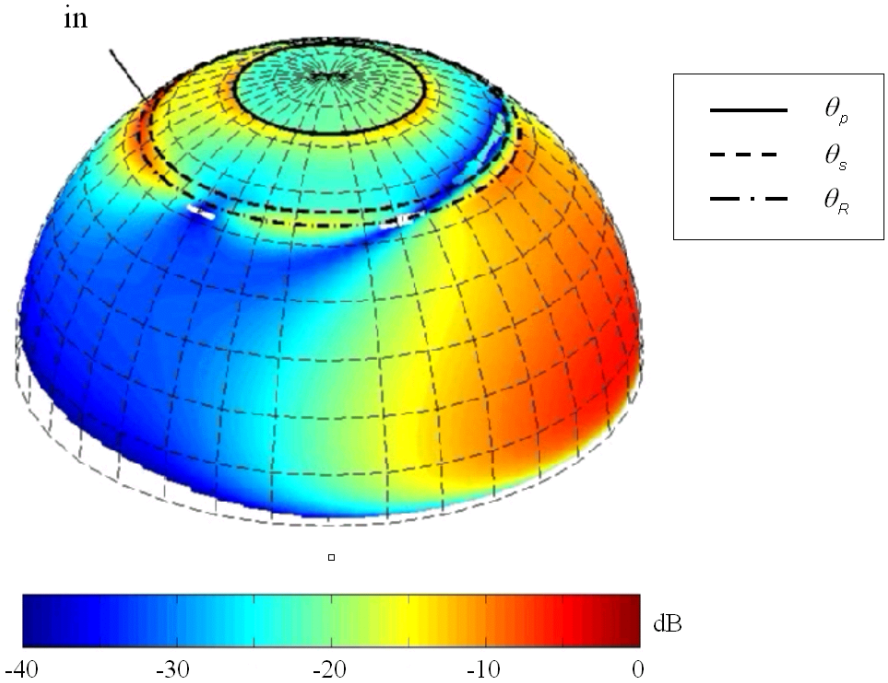

Figure 6. A $\sigma(\theta_{\mathrm{out}},\phi)$ prediction for rough basalt at 3.5 kHz for $\theta_{\mathrm{in}} = 52.5^{\circ}$ (near the Rayleigh angle, θ_{R}). The straight line marked "in" (upper left) indicates the incident direction. Decibel levels of σ are rendered in color on the "northern hemisphere" of a unit sphere. The "latitude" is θ_{out}, and the "longitude" (relative to incident) is ϕ. The grid spacing for both is 10°.

3.4 Computational Speed

The scattering algorithm is vectorized over all the in/out angles in order to achieve greater computational speed. The calculations for this article were all done in Matlab on an ordinary two year old PC workstation[#]. In Fig. 2, the computations were vectorized over 881 grazing angle values [$\theta = (1.0^o, 1.1^o, \ldots, 89.9^o, 90.0^o)$], and each small-slope curve required 0.3 sec of computation time. In Fig. 6, there are seventy-nine θ_{out} values and seventy-three ϕ values, for a total of 13,067 scattering directions. The figure was produced in a single vectorized computation requiring 11.5 sec.

4 CONCLUSIONS

We have developed an algorithm for the rapid, accurate calculation of the acoustic scattering strength of an elastic medium with a random surface that has a power-law roughness spectrum. The physical basis is the small-slope theory of scattering—a generalization of perturbation theory that does not assume the roughness to be small relative to a wavelength. The algorithm's output compares favorably with perturbation calculations, and we have used it to perform a geoacoustic inversion with at-sea experimental data. We are beginning a series of controlled laboratory experiments to fully validate the algorithm and to examine some of its specific predictions.

5 ACKNOWLEDGEMENT

This work was supported by the U.S. Office of Naval Research.

6 REFERENCES

1. A. Ishimaru, *Wave propagation and scattering in random media*, Academic Press, 1978.
2. T. Jenserud, D. Simons, and X. Cristol, "Rumble Project—Scattering Index Models," Norwegian Defence Research Establishment Report 2001/03685, September 2001.
3. P. D. Mourad and D. R. Jackson, "A model/data comparison for low-frequency bottom backscatter," J. Acoust. Soc. Am. 94, 344–358 (1993).
4. D. R. Jackson, D. P. Winebrenner, and A. Ishimaru, "Application of the composite roughness model to high-frequency bottom backscattering," J. Acoust. Soc. Am. 79, 1410–1422 (1986).
5. H.-H. Essen, "Scattering from a rough sedimental seafloor containing shear and layering," J. Acoust. Soc Am. 95, 1299–1310 (1994).
6. A. G. Voronovich, "Theory of sound scattering by a free corrugated surface", Sov. Phys. Acoust. 30, 444–448. (1984).
7. A. G. Voronovich, "A unified description of wave scattering at boundaries with large and small roughness" in *Progress in Underwater Acoustics*, edited by H. M. Merklinger (Plenum, New York, 1986), pp. 25–34.
8. R. Dashen and D. Wurmser, "A new theory for scattering from a surface," J. Math. Phys. 32, 971–985 (1991).
9. D. Wurmser, "A manifestly reciprocal theory of scattering in the presence of elastic media," J. Math. Phys. 37, 4434–4447 (1996).

[#] Two 800 MHz processors, 500 MB physical memory.

10. R. F. Gragg, D. Wurmser, and R. C. Gauss, “Small-slope scattering from rough elastic ocean floors: General theory and computational algorithm”, J. Acoust. Soc. Am. 110, 2878–2901 (2001).
11. J. A. Oglivy, *Theory of scattering from random rough media,* Adam Hilger, 1991.
12. R. Dashen, F. S. Henyey, and D. Wurmser, “Calculations of acoustic scattering from the ocean surface,” J. Acoust. Soc. Am. 88, 310–323 (1990).
13. R. J. Soukup and R. F. Gragg, “Backscatter from a limestone seafloor at 2–3.5 kHz: Measurements and modeling,” J. Acoust. Soc. Am. 113, 2501–2514 (2003).
14. N. C. Makris, L. Z. Avelino, and R. Menis, “Deterministic reverberation from ocean ridges,” J. Acoust. Soc. Am. 97, 3547–3574 (1995). (Specifically, our analysis of Mid-Atlantic Ridge bathymetry measurements that are described therein.)
15. D. M. Drumheller and R. F. Gragg, “Numerical evaluation of an integral found in the theory of scattering from rough interfaces,” Naval Research Laboratory Memorandum Report 7140–00–8436, 17 March 2000.
16. D. M. Drumheller and R. F. Gragg, “Evaluation of a fundamental integral in rough-surface scattering theory,” J. Acoust. Soc. Am. 110, 2270–2275 (2001).
17. W. H. Press, B. P. Flannery, S. A. Teukolsky and W. T. Veterling, *Numerical Recipes*, Cambridge University Press, 1986.
18. D. M. Drumheller, “Padé approximations to matched filter amplitude probability functions,” IEEE Trans. Aerosp. Electron. Syst. 35, 1033–1044 (1999).
19. R. J. Soukup and P. M. Ogden, “Bottom Backscattering Measured Off the South Carolina Coast During Littoral Warfare Advanced Development Focused Technology Experiment 96-2,” Naval Research Laboratory Memorandum Report 7140–97–7905, Washington, D.C., April 28, 1997.
20. R. J. Soukup, “Bottom Backscattering Measured Off the Carolina Coast During the Littoral Warfare Advanced Development System Concept Validation Experiment 97 (LWAD SCV 97),” Naval Research Laboratory Report 7140–98–9885, Washington, D.C., June 15, 1998.
21. E. L. Kunz, “Bottom Backscattering Measured Off the Carolina Coast During the Littoral Warfare Advanced Development 98-4 Experiment,” Naval Research Laboratory Memorandum Report 7140–99–8339, Washington D.C., February 26, 1999.
22. “Session 1pAO, Acoustical Oceanography, Underwater Acoustics and Signal Processing in Acoustics: Geoacoustic Inversion I,” J. Acoust. Soc. Am. 113, No. 4, Pt. 2, 2189–2192 (2003).
23. G. Caviglia and A. Morro, *Inhomogeneous waves in solids and fluids*, World Scientific, 1992.